Patterned graphene on SiN waveguides for mode locking of fiber lasers

Goran Kovacevic[1], Takuma Shirahata[1], Bingchang Wu[1], Pengtao Yuan[1], Ting-Hui Xiao[2], Lei Jin[1], Taiki Inoue[3], Shigeo Maruyama[3,4], Zhenzhou Cheng[2], Sze Y. Set[1], and Shinji Yamashita[1]

[1]*Research Center for Advanced Science and Technology (RCAST), The University of Tokyo, 4-6-1 Komaba, Meguro-ku, Tokyo 153-8904, Japan*

[2]*Department of Chemistry, The University of Tokyo, 7-3-1 Hongo, Bunkyo-ku, Tokyo 113-0033, Japan*

[3]*Department of Mechanical Engineering, The University of Tokyo, 7-3-1 Hongo, Bunkyo-ku, Tokyo 113-8656, Japan*

[4]*Energy NanoEngineering Laboratory, National Institute of Advanced Industrial Science and Technology (AIST), 1-2-1 Namiki, Tsukuba 305-8564, Japan*

[*]E-mail: gorank@cntp.t.u-tokyo.ac.jp, syama@cntp.t.u-tokyo.ac.jp

In this paper, we report our results on the use of patterned graphene on SiN waveguides inside an erbium doped fiber ring laser cavity for passive mode locking. We confirm the dominant influence of graphene over non-linear polarization rotation (NPR), arising from polarizing fiber to chip grating couplers, by observing the limits of NPR in high cavity loss fiber lasers. We fabricated waveguides, transferred and patterned graphene to three different lengths, and observed different types of pulses based on the length of graphene, pump power and polarization state of the cavity. We confirmed the success of graphene processing through Raman scattering and saturable absorption measurements, as well graphene absorption simulation. High chip-coupling loss was overcome by using multiple erbium-doped fiber amplifiers. We believe this research will stimulate further interest in combining integrated photonics and fiber laser technologies, and the miniaturization of pulsed laser cavities.

1. Introduction

Fiber lasers, based on fiber cavities and fiber-based amplifiers, have seen a tremendous growth in recent years in both the academia as well as industry. Mode locked fiber lasers are pulsed lasers with a broad optical spectrum achieved through saturable absorption (passive) or cavity gain/loss modulation (active) and they have been applied in micromachining[1,2], laser marking[3], gas sensing[4] and non-linear applications, like the supercontinuum generation[5-7] and light detection and ranging (LIDAR)[8,9]. The high interest in mode locked fiber lasers is mostly due to their ease of fabrication, compactness and highly stable operation, which makes them inherently superior to the solid-state lasers in a wide area of applications.

In addition to fiber lasers, there has also been an increased interest in producing lasers, and pulsed lasers, with integrated photonic components combined with fibers, III-V reflective semiconductor optical amplifiers (RSOAs) and other active materials. This interest was sparked by the laser source requirements of on-chip optical interconnects but has been extended to utilizing the non-linearities of optical chips in novel ways. Silicon nitride (Si_3N_4, abbreviated as SiN) waveguides have been used in combination with III-V components to generate ultra-narrow line-width lasers[10,11] and in combination with fibers it was demonstrated that SiN resonators can be used to generate frequency combs[12,13]. Even with these advancements, there is limited research interest in fiber ring laser cavities, where a photonic chip is integrated inside the cavity path, which we believe is due to the high cavity loss induced by chip coupling. In this paper, we show the mode-locking properties of SiN waveguides covered with patterned 2D material graphene, which are integrated inside the fiber laser cavity. We overcome the high intra-cavity loss issue by utilizing two or three erbium-doped fiber amplifiers (EDFAs), depending on the length of graphene.

Graphene is a 2D material consisted of carbon atoms arranged into a honey-comb lattice[14]. As such it has many unique electronic and optical properties[15,16], like high carrier mobility and wavelength independent absorption[17], which made it suitable in wide range of integrated optical devices, like modulators[18,19], photodetectors[20] and polarizers[21]. It also has unique non-linear properties which have been extensively studied, and most significantly for fiber lasers it is an excellent saturable absorber due to the Pauli blocking principle[22]. Many graphene-based mode-locked fiber lasers have been studied previously[23-27], but they mostly consisted of graphene covering fiber ferrules, or being a part of fiber connectors, thus

having light inside the cavity travel perpendicular to the graphene sheet, which limits the interaction length. There have also been all-fiber graphene mode locked lasers, where graphene was placed on top of tapered fibers[28] or D-shaped fibers[26,29], thus having light travel parallel to the graphene sheet, and increasing interaction length. In our work, we place, and pattern, graphene on top of SiN waveguides, thus taking advantage of strong light confinement inside the waveguides and increased interaction length due to the light traveling parallel to the graphene sheet (the interaction length in our integrated approach is still a few orders of magnitude smaller than in "parallel incidence" fiber setups). Our work shows the potential of miniaturizing mode-locked laser cavities, by utilizing ultra-short, integrated saturable absorbers.

The only previous report, to the best of our knowledge, related to the use of graphene with integrated photonics for fiber laser mode locking is the one by Wong, et al,[30] in which graphene covered Si waveguides were used to mode lock a fiber laser. However, that report doesn't discuss the influence of different lengths of graphene on mode locking, or the influence of non-linear polarization rotation (NPR)[31]. To couple light into the chip, we utilize focusing diffraction gratings, which are highly polarization dependent, thus effectively introducing a polarizer inside the cavity path. If the cavity is consisted of standard single mode fibers, as is the case in our setup and previous reports, the polarizer can induce NPR-based mode locking[31]. In this work, we performed detailed experimental characterization of NPR mode locking in high intra-cavity loss fiber lasers without graphene, where we inserted an in-line polarizer and a variable attenuator in the cavity to simulate chip coupling loss and concluded that NPR cannot mode lock a cavity beyond 20 dB intra cavity loss. This deterministically proves that graphene is responsible for mode-locking in the chip-fiber cavity, as the cavity loss induced by the SiN chip in our setup was between 20 dB and 30 dB depending on the graphene length. However, we believe mode locking is triggered by a combined influence of graphene and NPR based on the similarities of the optical spectra, and its dependency of the cavity polarization state. The fact that we can deterministically prove that graphene is responsible for mode locking opens the path for using graphene covered waveguides in more compact, or all-integrated, pulsed laser setups. The use of SiN also has an advantage over Si as there is no two-photon absorption[32], which was shown to influence pulse shaping in laser cavities[33].

There was recently an increased interest in combining free-space graphene optical modulators with fiber laser cavities for Q-switching[34], as well as active mode locking[35] applications. Our work perfectly complements and follows up on these reports, as we show that it is possible to utilize graphene enhanced integrated photonics for fiber laser mode locking, which is ideal for creation of graphene modulators or even more complex graphene-based systems. Our work, along with the previous reports, shows the potential of creating actively and passively mode locked lasers using graphene enhanced chips, along with the miniaturization of fiber laser cavities.

The results of this paper have been partly submitted to two conference proceedings[36,37], and this paper presents the combination of them with additional experimental, numerical and qualitative discussions. The following chapter on "Experimental Methods" will introduce the basic devices we fabricated and used in experiments, i.e. the patterned graphene covered SiN waveguides, characterization of graphene through linear and saturable absorption as well as the Raman response, and the fiber laser cavities used for the main mode locking experimental results. The final chapter on "Results and Discussion" will introduce the mode locking results for different lengths of graphene and different pump powers. We obtained different types of pulses based on different lengths of graphene, with respect to pulse width and the harmonic order, all of which will be discussed in that chapter. We conclude the paper with the summary of the research and potential future plan and applications.

2. Experimental methods

The patterned graphene covered SiN waveguide used in experiments is presented in Fig. 1. It is a ridge waveguide made in a SiN wafer of thickness $d_{SiN} = 720\ nm$, with an etch depth of $d_{Etch} = 400\ nm$. The width of the waveguide is $w_{WG} = 1.2\ \mu m$, and SiN is on top of a silica box layer. The cross section of the device, with all the parameters, is presented in Fig. 1(b). Waveguides were fabricated using e-beam lithography and plasma etching. To couple light into, and out of the waveguide, we used focusing diffraction gratings[38], optimized for the TE mode, and standard single mode fibers. The TE mode of the waveguide, with emphasized graphene, is presented in Fig. 1(c).

We used single-layer, chemical vapor deposition (CVD) grown, commercial graphene on copper foil and transferred it to our SiN waveguides using the standard PMMA wet

transfer method[39,40]. To pattern graphene, we used a negative resist HSQ and e-beam lithography in the following special procedure: We first spin-coated a buffer layer of PMMA, on top of which we spin coated HSQ and performed e-beam lithography and development steps to form the protective lines, corresponding to the graphene patterns. We then performed 10 minutes of O_2 plasma to etch the buffer layer of PMMA and graphene outside of the protective lines. The purpose of the PMMA buffer layer is to enable the removal of HSQ through a lift-off process, as the standard way of HSQ removal in the HF acid could have damaged our waveguides. This is how the 100 μm and 150 μm patterns were fabricated, as shown in Fig. 2(a,b). However, as we removed the HSQ through the PMMA lift-off in acetone, we discovered that the lift-off also removed graphene underneath the HSQ lines. We believe this is due to the fact that we used long HSQ lines which covered multiple waveguides, thus creating additional strain and causing removal of graphene. This is how we obtained the 400 μm graphene pattern, as we wanted to remove HSQ due to misalignment, but discovered that graphene was removed underneath the HSQ, and around the gratings, which was beneficial. We initially conducted all the experiments with the 400 μm pattern, after which it was removed in O_2 plasma, and a new layer of graphene was transferred, repeating the patterning procedure to obtain 100 μm and 150 μm patterns. In the latter case we didn't remove the PMMA/HSQ stack, so graphene wouldn't be damaged, and performed experiments with it, but it can be assumed that the results wouldn't change significantly based on PMMA/HSQ removal as its low refractive index doesn't heavily influence the optical mode. The waveguides with grating couplers and HSQ lines which form the graphene pattern are shown in Fig. 2. In Fig. 2(a) we show the detailed steps of graphene patterning with a PMMA/HSQ stack and O_2 plasma, as explained in this paragraph.

To confirm single layer graphene was used, we performed Raman spectral response measurements. Due to the strong spectral response of SiN, it is not feasible to observe the spectral response of graphene on a SiN chip directly. To estimate its Raman spectral response, in the same graphene transfer process as the SiN chip we also transferred graphene onto two silica dummy substrates, one before, and one after the SiN chip (we used three pieces of graphene, where at the last step of the transfer the first and the third were used for silica, while the second was used for SiN). We measured the Raman response from these two silica substrates, and in both (in both the cases of the 400 μm pattern, and the 100 μm and 150 μm

patterns), we could observe the spectrum shown in the Fig. 3. The clearly higher 2D peak (with respect to the G peak) implies a successful single graphene layer transfer[41], and we can conclude that the same graphene is utilized on the SiN chips, as the transfer was done in the same process.

Since we patterned graphene to obtain its different lengths (L, as per Fig. 1(a)) that cover SiN waveguides, we could estimate the graphene absorption through the cut-back method. Due to the small sample the result is not of high accuracy, but it could give us information on the success of the graphene transfer and graphene's light matter interaction properties. We used a CW laser source with a 1560 nm wavelength coupled into the waveguide through the gratings using a regular SM fiber, with the coupling efficiency optimized through a polarization controller existing in front of the chip. The light from the SiN waveguide was outcoupled into another SM fiber and power was observed through a photodetector. We observed average coupling losses of 21 dB, 22.5 dB and 29.2 dB for the graphene lengths of 100 μm, 150 μm and 400 μm, respectively, and 17.2 dB when there is no graphene, implying the graphene absorption rate of 0.033 dB/μm (the 400 μm length loss is undervalued as it is for open-clad graphene pattern for which the TE mode is more confined inside the wavegude (Fig. 1(c))). We also confirm the graphene absorption by performing a 2D FEM optical mode simulation of the graphene covered SiN waveguide using the COMSOL Multiphysics software. Graphene is taken into account through its 2D surface dynamic optical conductivity $\sigma = 60\ \mu S$, and magnetic field boundary conditions[42], which are incorporated in the COMSOL simulation through surface currents. This approach certifies that graphene only interacts with electric fields parallel to its sheet. Graphene is assumed to cover the waveguide as presented in Fig. 1. It is reasonable to assume that graphene breaks around the ridge and falls onto the bottom surface of the SiN wafer around it, due to multiple post processing steps required for graphene patterning. With these assumptions, and assuming the PMMA cladding, we used COMSOL to obtain the complex propagation wavevector of the optical mode β, and assuming the power dependency as $P_{Out} = P_{In}\exp(-2Im(\beta)L)$, where L is the length of graphene, we obtain the graphene absorption rate of 0.032 dB/μm. This is in very high accordance with the experimental value of 0.033 dB/μm as shown in Fig. 4 where we plotted the experimental values along with the simulation linear curve starting from the "no graphene" coupling loss. This confirms that the

linear loss is due to graphene, and that patterning was successful. The optical mode obtained with this simulation is the one shown in Fig. 1(c).

Very important parameter for passive laser mode locking is the saturable absorption (SA) of the material. Saturable absorption is the property of materials that when the input peak power increases, it leads to a decay in the material's absorption, which is very pronounced in graphene as detailed in the introductory chapter. We characterized the SA properties of our patterned graphene on SiN waveguides, and the results are shown in Fig. 5. We used a commercial pulsed laser at 1560 nm central wavelength, and a variable attenuator to tune the input power of the SiN chip. We also used a 90/10 power splitter in front of the chip so we could monitor the input power in real time, and obtain the transmission curve, with respect to the input power. From the results in Fig. 5, we could clearly observe the SA characteristics of different lengths of graphene, thus confirming it's potential for mode locking of fiber lasers. To confirm the pulsed laser curves are the result of graphene's SA, we performed the same experiment with the use of a CW laser instead of the pulsed one, which has a flat peak power and should not induce SA. Indeed, the results in the case of the CW laser seem random, confirming the impact of graphene. We didn't use any EDFA to amplify the pulsed laser in front of the variable attenuator, so could only observe the beginning of the SA curve. However, even though the SA seems to be only a fraction of the percent, this is due to the high coupling loss of the chip and if it is normalized to the output power we can observe that the influence of the SA is in the range from 10% to the 20% of the output power. In fact, the largest graphene length seems to imply strongest SA if normalized to the output power (around 20%), but the penalty is paid in the high insertion loss. This is in accordance to previously published studies[43].

Finally, we introduce the fiber laser experimental setup, to which we integrated the patterned graphene covered SiN chip, shown in Fig. 6(a). It is a typical fiber ring cavity, with two or three EDFAs depending on the length of graphene. In Fig. 6(a) "EDFAs" refer to commercial EDF amplifiers we used, while 980 nm pump and the EDF correspond to our custom-made amplifier. We utilized 25m of EDF to compensate for the chip coupling loss and amplify the signal as much as possible prior to the chip coupling. We also used 2 polarization controllers (PCs), one in front and one after the chip. This is similar to NPR based fiber lasers, and indeed we optimized the cavity, so we can clearly observe the effects

of both NPR and graphene. The total length of the cavity is around 240 m, corresponding to a fundamental frequency of around 900 kHz. Such long cavity is induced by 150m of extra SMF we introduced and the pigtails of fiber components (the length of the waveguide is only around 490 μm). The reason for the long cavity length is two-fold: One reason is to offset the large normal dispersion of multiple EDFAs, thus making the average dispersion of our cavity anomalous (D=2.16 ps/nm). The other reason is to amplify the NPR effect, and we show that the mode locking is the result of combined influence of both graphene and NPR. However, it is also critical to show that NPR was not responsible for mode locking on its own, as we explained in the introductory chapter. To achieve that, we made a fiber laser cavity with an in-line fiber polarizer, and a variable attenuator to simulate the chip coupling loss, as presented in Fig. 6(b). The only difference between Fig. 6(a) and Fig. 6(b) are the polarizer and attenuator instead of the chip. Using this setup, we could establish the influence, and limits, of NPR, that helped us realize the influence of patterned graphene. The experimental results are presented in the next chapter.

3. Results and discussion

In this chapter, we present the mode locking results of the fiber lasers. We first introduce the results for the longest length of graphene, 400 μm, followed by 100 μm and 150 μm graphene lengths, for different pump powers. We conclude the chapter with the mode locking results through solely NPR and compare it with mode-locking with graphene patterned SiN chip. We show that it is possible to obtain single harmonic, ps pulses, but also ns pulses, with pump power and PC state optimization. We show that it is not possible to mode lock the fiber laser by using solely NPR for fiber laser cavities with beyond 20 dB intra-cavity loss, and that NPR generally produces longer pulses in comparison to the graphene patterned chip. All optical spectra are obtained using an Optical Spectrum Analyzer (OSA) with resolution of 0.05 nm, RF spectra using an RF spectrum analyzer with 1 kHz resolution and a photodetector of 1 GHz bandwidth was used.

3.1 Mode locking using the 400 μm graphene pattern

In this section we introduce the results of the 400 μm long graphene pattern on the SiN waveguide, shown in Fig. 2(c), using the mode locking setup from Fig. 6(a). Due to the high coupling loss owed to the long graphene length, measured as 29.2 dB, we used all three

EDFAs to compensate for the loss. Mode locking was achieved by changing the state of the PC, and the results are presented in Fig. 7, which shows the optical and the RF spectrum with the oscilloscope trace. Obtaining of the soliton optical spectrum by changing the state of the PC is similar to the case of NPR mode locking, which leads us to believe NPR has an influence on the pulse. Also, it should be noted that obtaining a pulse proved to be difficult in this configuration, but once it was reached it showed stable operation.

In the case of the 400 μm long graphene length, we were unable to obtain a fundamental harmonic pulse, and we could only observe 3rd and 5th harmonics, the results for the latter shown in Fig. 7. Different harmonics were obtained by shifting the state of the PC, while changing (reducing) pump power showed no influence on the pulse. We performed an autocorrelation measurement of the pulse as well and could observe that the pulse width is 3.37 ps, as shown in Fig. 8, assuming a sec^2 soliton pulse shape.

3.2 Mode locking using the 100 μm graphene pattern

In the case of the 100 μm long graphene that induced around 21 dB loss (Fig. 2(a)), we could use only 2 EDFAs, as per Fig. 6(a). One is the custom made 25 m EDF with a 980 nm pump, and the other is a commercial EDFA. In the case of the custom EDF, we held the pump power to a constant high value due to the length of the doped fiber, while we optimized the pump power of the commercial EDFA.

Under high pump power of the commercial EDFA, it was very easy to find soliton pulses by changing the state of the PC. However, most of the pulses obtained were highly multi-pulsed. One characteristic example is presented in Fig. 9. We were able to measure the autocorrelation trace of the pulse and observe that the pulse width is similar to the case of the long graphene length, measured as 3.51 ps (Fig. 10).

By optimizing the pump power of the commercial EDFA, and further changing the state of the PC, we were able to obtain fundamental harmonic pulses, as shown in Fig. 11. Due to the reduced power we were unable to obtain the autocorrelation trace, but we can observe that the optical spectrum is similar to the one obtained for high pump power so we can conclude it possesses a similar pulse width of approximately 3 ps. In the case of the optimized pump power, we could also observe broader pulses with the fundamental frequency and a narrow optical spectrum, by changing the state of the PC. Similar pulses were obtained with a 150 μm, and a typical example will be shown in the next section.

3.3 Mode locking using 150 μm graphene pattern

Lastly, we introduce the results in the case of the 150 μm graphene length, covering the SiN waveguide. In this case, we use 2 EDFAs like in the case of the 100 μm graphene length and only focus on the results in the case of optimized pump power.

As mentioned in the previous paragraph, in both the cases of 100 μm and 150 μm graphene length we were observing a broad pulse with a unique optical spectrum, and a typical example is shown in Fig. 12. The oscilloscope trace implies a 160 ns pulse width, substantiated by a decaying RF spectrum (in log scale). By examination of the optical spectrum, we can observe a characteristic CW peak, which we believe is responsible for pulse broadening and is a result of the influence of grating couplers. For the purpose of compactness of the manuscript, we don't show all the spectra we obtained, but can state that an even stronger CW instability could have been observed in our experiments, with multiple sharp peaks around the central wavelength of the soliton, resulting in even broader pulses. Grating couplers induce strong reflections, and with the 490 μm length of the waveguide they form a Fabry-Perrot (FP) cavity of the Free Spectral Rage (FSR) of 1.2 nm, which makes mode locking complex. We believe the strong CW peaks are the result of the longitudinal modes of the FP cavity, but even so, graphene's SA is enough to lock them into a soliton pulse. Interestingly, Bogustawski, et al, observed similar CW peaks in their spectra, in the case of the actively mode locked fiber laser using an external graphene modulator[35]. This implies that the effect could be a result of some fundamental physical property of graphene, but we leave its full characterization for future work.

Like in the case of the 100 μm graphene length, we could also observe the single short pulse operation, with the results shown in Fig. 13. As before, we were unable to measure the autocorrelation trace, but can estimate the pulse width of approximately 3 ps based on the spectral widths and previous results. By comparing the results from Figs. 12 and 13, we can observe that the main difference is the CW instability, and the spectrum in Fig. 13. is generally cleaner. The only difference in the state of the cavity is the sate of the PC, i.e. by tuning the PC we could switch between the operations shown in Figs. 12 and 13. This implies that we can control the width and energy of the output pulses, based on the properties of graphene SA and the influence of grating couplers, which could be useful in high pulse energy applications.

This concludes our results of the patterned graphene mode locking, using the cavity shown in Fig. 6(a). We summarize our results in Table I where we show the performance metrics we obtained for different lengths of graphene. In Table I, we include the values obtained in the case of fundamental mode locking for graphene lengths of 100 μm and 150 μm, and the only multi-pulsed result obtained in the case of the 400 μm length. From the table, we can observe a similar performance of the laser between different graphene lengths which we believe is due to the limits of NPR, but smaller graphene lengths with lower insertion loss are much more feasible for commercial use.

Before concluding the paper, we realize it is critical to estimate the influence of NPR on mode locking and provide quantitative proofs that it is truly graphene which is responsible for mode locking and not NPR. In the following section, we provide our results for mode locking using NPR with high intra cavity loss, and without graphene, showing that it is not possible to mode lock a laser beyond 20 dB of intra cavity loss by using only NPR, thus confirming the influence of graphene.

3.4 Mode locking using only NPR for different values of intra-cavity loss

To confirm the influence of NPR, we developed the fiber laser cavity shown in Fig. 6(b). It is a typical NPR cavity, where an in-line fiber polarizer is inducing mode locking due to the non-linear Kerr effect. One of the main challenges of introducing a chip into the cavity is the high intra cavity loss, so to simulate the high loss we also introduce a variable attenuator. The idea is to replicate the conditions of the cavity with the chip by using only fiber components, so we can estimate the influence of NPR in the best-case scenario. We tuned the PC state of the cavity to obtain a mode-locked spectrum, and the spectral results for different intra-cavity losses are presented in Fig. 14. We overcame the losses by using 1, 2 or 3 EDFAs, like in the case of the “chip-cavity”, and we even attempted to add additional DSF fiber for high cavity losses to induce additional non-linearity that could potentially mode-lock the pulse.

Our main result, shown in Fig. 14, is that we were unable to mode lock the cavity, shown in Fig. 6(b), when the loss of the attenuator was greater than 20 dB. The intra-cavity loss of 20 dB was the highest for which we could observe a soliton optical spectrum, shown in Fig. 14(h). Considering that even for the smallest length of graphene, the chip coupling loss was 21 dB, we conclude that the pulses we obtain using the graphene covered chip are

indeed due to the influence of graphene. However, the similarities of the spectral shape and width, as well as the fluctuation of the central wavelength with PC variation, lead us to believe that NPR indeed has influence on the mode-locking even when graphene covered waveguides are present. Also, in the case of the NPR cavity, for some soliton spectra we couldn't observe the pulse on the oscilloscope (like in the case of the 20 dB loss), which we believe is due to the high noise of the pulse. In the case of graphene, pulses were always observed even for higher intra-cavity losses.

Since the characterization of high-intra cavity loss cavities is not common in literature (the losses are usually minimized inside the cavity), we also performed numerical mode-locking simulations using the standard split-step Fourier method[44], and assuming the NPR can be modelled like a standard SA as[45]:

$$T = 1 - T_{SA}\frac{1}{1+\frac{P}{P_{Sat}}}. \qquad (1)$$

In the previous equation, T_{SA} is the saturable transmission, P_{Sat} is the saturation power and P is the power of the pulse. By changing the saturable transmission, and keeping the saturation power constant, we could confirm the shape of the high loss spectra, also shown in Fig. 14. The main purpose of the simulation was to confirm the pulse optical spectra under high intra cavity loss condition.

Experimentally, for lower intra-cavity loss, it was easier to observe pulses on the oscilloscope, as well as the autocorrelation trace, and for a 10 dB intra cavity loss the results are shown in Fig. 15. Interestingly, the pulse width is 4.52 ps, which is longer than the pulses obtained using the patterned graphene, implying that graphene influences pulse shortening.

With these insights in mind, we also attempted to mode lock the chip cavity in Fig. 6(a), by using chips that are not covered with graphene, when the loss of the chip is around 17 dB. Even though this loss is smaller than 20 dB, we were unable to observe any mode locked optical spectra, but we could observe very high CW instabilities and multiple modes. We believe these modes are the result of the Fabry-Perrot cavity induced by the waveguide and grating couplers, and they limit the mode locking possibilities. However, as our results show, graphene can stabilize these modes, and lock them, through its dominant saturable absorption.

4. Conclusions

In conclusion, in this paper we have shown the fiber ring laser mode locking properties, and possibilities, using intra cavity patterned graphene on SiN waveguides. We have observed two types of pulses, ns and ps, and explained qualitatively the differences in pulses, arising from the high reflectivity of fiber-to-chip grating couplers. The high loss of the cavity, induced by the high chip coupling loss, was overcome by using multiple EDF amplifiers. The grating couplers, in addition to their high reflectivity, are also polarization dependent, making them an effective polarizer, which can trigger NPR mode locking. To prove that graphene is indeed influencing mode locking, we designed a high intra-cavity loss fiber ring cavity for NPR mode locking and proved that mode locking is not feasible with only NPR beyond 20 dB intra cavity loss. Considering that the patterned graphene covered chip induces losses between 21 dB and 30 dB, we could deterministically prove that graphene is truly responsible for mode locking, but believe the entire mechanism is a combination of graphene and NPR.

In this paper, we focused on the worst-case scenario in terms of losses and proved experimentally that mode locking is possible under very high intra cavity loss by utilizing patterned graphene on a SiN chip. For practical purposes, reduction of cavity loss would be desired to reduce the required pump power and energy consumption, which could be accomplished by optimizing the grating coupling efficiency[46,47] or further reducing the length of graphene. Even though low cavity loss is desired, the research field of high pump power lasers is highly developed through the research related to high output power lasers[48], where special doped fibers could be utilized to reduce the length of the gain fiber and optimize the cavity. Similar principles could be applied to optical chip-enhanced fiber laser cavities even under high cavity losses with the goal of miniaturizing the cavity and potentially creating chip compatible laser sources.

We believe our results will spark further interest in using optical chips integrated inside fiber laser cavities, for mode locking, but also filtering or signal processing purposes. Furthermore, we believe it could also spark interest in the miniaturization of fiber laser cavities, where the entire cavity could be chip-based, with graphene as a SA absorber for mode locking, and only using fiber-based amplifiers inside the cavity. This could open a path to ultra-high frequency fiber lasers, and this is a part of our future work.

Acknowledgments

The authors would like to acknowledge the financial support of the Japanese Society for Promotion of Science through the JSPS KAKENHI Grant numbers 16H00902 and JP15H05760, as well as of the DC2 Grant-in-Aid for JSPS Fellows number 201709162 and the Global Leader Program for Social Design and Management (GSDM) of the University of Tokyo. The authors would also like to acknowledge that the graphene patterning recipe, using HSQ and a PMMA buffer layer, was originally developed by the Lipson group of the Columbia University in New York, and optimized by G.K. The fabrication was conducted at the Center for Nano Lithography and Analysis and the VLSI Design and Education Center (VDEC) of the University of Tokyo.

References

1) M. Malinauskas, A. Zukauskas, S. Hasegawa, Y. Hayasaki, V. Mizeikis, R. Buividas, and S. Juodkazis, Light: Science & Applications **5**, e16133 (2016).
2) T. Tamaki, Opt. Express **14**, 10461 (2006).
3) W. Shi, Q. Fang, X. Zhu, R. A. Norwood, N. Peyghambarian, Appl. Opt. 53, 6554 (2014).
4) G. Whitenett, G. Stewart, H. Yu, B. Culshaw, J. Lightwave Technol. 22, 813 (2004).
5) J. Takayanagi, N. Nishizawa, Jpn. J. Appl. Phys. 45, L441 (2006).
6) S. Kim, J. Park, S. Han, Y.-J. Kim, and Seung-Woo Kim, Opt. Lett. 39, 2986 (2014).
7) Y.-X. Guo, X.-H. Li, P.-L. Guo, and H.-R Zheng, Opt. Express 26, 9893 (2018).
8) W. C. Swann, and N. R. Newbury, Opt. Lett. 31, 826 (2006).
9) M. U. Piracha, D. Nguyen, D. Mandridis, T. Yilmaz, I. Ozdur, S. Ozharar, and P. J. Delfyett, Opt. Express 18, 7184 (2010).
10) Y. Fan, J. P. Epping, R. M. Oldenbeuving, C. G. H. Roeloffzen, M. Hoekman, R. Dekker, R. G. Heideman, P. J. M. van der Slot, K.-J. Boller, IEEE Photonics Journal 8, 1505111 (2016).
11) B. Stern, X. Ji, A. Dutt, M. Lipson, Opt. Lett. 42, 4541 (2017).
12) C. Joshi, J. K. Jang, K. Luke, X. Ji, S. A. Miller, A. Klenner, Y. Okawachi, M. Lipson, and A. L. Gaeta, Opt. Lett. 41, 2565 (2016).
13) C. Joshi, A. Klenner, Y. Okawachi, M. Yu, K. Luke, X. Ji, M. Lipson, and A. L. Gaeta, Opt. Lett. 43, 547 (2018).
14) K. S. Novoselov, A. K. Geim, S. V. Morozov, D. Jiang, Y. Zhang, S. V. Dubonos, I. V. Grigorieva and A. A. Firsov, Science 306, 666 (2004).
15) A. K. Geim and K. S. Novoselov, Nat. Mater. 6, 183 (2007).
16) S. Sato, Jpn. J. Appl. Phys 54, 040102 (2015).
17) R. R. Nair, P. Blake, A. N. Grigorenko, K. S. Novoselov, T. J. Booth, T. Stauber, N. M. R. Peres and A. K. Geim, Science 320, 1380 (2008).
18) M. Liu, X. Yin, E. Ulin-Avila, B. Geng, T. Zentgraf, L. Ju, F. Wang and X. Zhang, Nature 474, 64 (2011).
19) M. Liu, X. Yin and X. Zhang, Nano Lett. 12, 1482 (2012).
20) X. Gan, R.-J. Shiue, Y. Gao, I. Meric, T. F. Heinz, K. Shepard, J. Hone, S, Assefa and D. Englund, Nat. Photonics 7, 883 (2013).
21) Q. Bao, H. Zhang, B. Wang, Z. Ni, C. Haley, Y. X. Lim, Y. Wang, D. Y. Tang and K. P. Loh, Nat. Photonics 5, 411 (2011).
22) S. Yamashita, J. Lightwave Technol. 30, 427 (2012).
23) Z. Sun, T. Hasan, F. Torrisi, D. Popa, G. Privitera, F. Wang, F. Bonaccorso, D. M. Basko, and A. C. Ferrari, ACS Nano 4, 803 (2010).
24) Q. Bao, H. Zhang, Z. Ni, Y. Wang, L. Polavarapu, Z. Shen, Q.-H. Xu, D. Tang, and K. Ping Loh, Nano Res. 4, 297 (2011).
25) Y. M. Chang, H. Kim, J. H. Lee, and Y.-W. Song, Appl. Phys. Lett. 97, 211102 (2010).
26) M. Jung, J. Koo, P. Debnath, Y.-W. Song, and J. H. Lee, Appl. Phys. Express 5, 112702 (2012).
27) A. Martinez, S. Yamashita, Appl. Phys. Lett. 101, 041118 (2012).
28) Y. Wang, W. Ni, S. Y. Set, and S. Yamashita, IEEE Photonics Technol. Lett. 29, 913 (2017).
29) J. D. Zapata, D. Steinberg, L. A. M. Saito, R. E. P. de Oliveira, A. M. Cardenas, E. A. Thoroh de Souza, Sci. Rep. 6(20644), 1 (2016).
30) C. Y. Wong, Z. Cheng, Z. Shi, Y. M. Chen, K. Xu, and H. K. Tsang, Proc. 10th Int. Conf. on Group IV Photonics, 2013, p. 35.
31) L. E. Nelson, D. J. Jones, K. Tamura, H. A. Haus, E. P. Ippen, Applied Physics B 65, 277 (1997).
32) R. Baets, A. Z. Subramanian, S. Clemmen, B. Kuyken, P. Bienstman, N. Le Thomas, G. Roelkens, D. Van Thourhout, P. Helin, and S. Severi, Proc. OFC Conf., 2016, Th3J.1.
33) E.-K. Tien, N. S. Yuksek, F. Qian, and O. Boyraz, Opt. Express 15, 6500 (2007).
34) D. Li, H. Xue, M. Qi, Y. Wang, S. Aksimsek, N. Chekurov, W. Kim, C. Li, J. Riikonen, F.

Ye, Q. Dai, Z. Ren, J. Bai, T. Hasan, H. Lipsanen, Z. Sun, 2D Meter. 4, 025095 (2017).
35) J. Bogustawksi, Y. Wang, H. Xue, X. Yang, D. Mao, X. Gan, Z. Ren, J. Zhao, Q. Dai, G. Sobon, J. Sotor, Z. Sun, Adv. Func. Meter. 1801539 (2018).
36) G. Kovacevic, T. Shirahata, P. Yuan, S. Set, S. Yamashita, Proc. CLEO Pacific Rim, 2018, 2981236 [Abstract accepted].
37) G. Kovacevic, T. Shirahata, B. Wu, T.-H. Xiao, L. Jin, T. Inoue, S. Maruyama, Z. Cheng, S. Y. Set, and S. Yamashita, Proc. Frontiers in Optics and Laser Science, 2018 [Abstract accepted].
38) J. Wang, Z. Cheng, Z. Chen, J.-B. Xu, H. K. Tsang, C. Shu, J. Appl. Phys. 117, 144504 (2015).
39) X. Li, W. Cai, J. An, S. Kim, J. Nah, D. Yang, R. Piner, A. Velamakanni, I. Jung, E. Tutuc, S. K. Banerjee, L. Colombo, R. S. Ruoff, Science 05, 1312 (2009).
40) A. Reina, H. Son, L. Jiao, B. Fan, M. S. Dresselhaus, Z. F. Liu, and J. Kong, J. Phys. Chem. C 112, 17741 (2008).
41) L. M. Malard, M. A. Pimenta,G. Dresselhaus, M. S. Dresselhaus, Physics Reports 473, 51 (2009).
42) G. Kovacevic, S. Yamashita, Opt. Express 20, 3584 (2016).
43) Z. Shi, C. Y. Wong, Z. Cheng, K. Xu, and H. K. Tsang, Proc. CLEO-PR, 2013, WA4-3.
44) G. Agrawal, Nonlinear Fiber Optics (Academic Press, Oxford, 2013), 5th ed., p. 47.
45) P. Wang, X. Xiao, H. Zhao, C. Yang, IEEE Photonics Journal 9, 1507008 (2017).
46) Yunhong Ding, Feihong Ye, Christophe Peucheret, Haiyan Ou, Yutaka Miyamoto, and Toshio Morioka, Optics Epxress 23, 3292 (2015)
47) C. Lacava, I. Cardea, I. Demirtzioglou, A.E. Khoja, Li Ke, D. J. Thomson, X. Ruan, F. Zhang, G.T. Reed, D.J. Richardson, and P. Petropoulos, Optics Express 25, 29798 (2017)
48) Michalis N. Zervas ; Christophe A. Codemard, IEEE JSTQE, 20 (2015).

Figure Captions

Fig. 1. (Color online) a) 3D scheme of a graphene covered SiN waveguide used for mode locking. b) 2D cross section of the waveguide with fabrication parameters. c) TE mode of the waveguide used in experiments and graphene absorption simulations.

Fig. 2. (Color online) a) Optical microscope of the waveguide with grating couplers and a 100 μm graphene pattern, including the intermediary patterning steps. b) 150 μm graphene pattern. c) 400 μm graphene pattern.

Fig. 3. (Color online) Raman spectral response of graphene on SiO_2 transferred in the same process as on the SiN chip, and a reference "no-graphene" SiO_2 spectrum (scaled).

Fig. 4. (Color online) Experimental results of the chip coupling loss and the graphene absorption simulation with respect to graphene length. The "0" graphene length corresponds to the average coupling loss before graphene transfer.

Fig. 5. (Color online) Transmission of the patterned graphene SiN waveguide using a pulsed and CW laser source in the case of a) 100 μm, b) 150 μm and c) 400 μm graphene patterns, showing saturable absorption (SA).

Fig. 6. (Color online) a) Fiber laser cavity with the patterned graphene SiN chip used for mode locking. b) High intra-cavity loss fiber laser cavity optimized for NPR mode locking.

Fig. 7. (Color online) Mode locking results in the case of the 400 μm graphene pattern. a) Optical spectrum and b) RF spectrum with oscilloscope trace inset.

Fig. 8. (Color online) Autocorrelation trace of the pulse obtained using a 400 μm graphene pattern.

Fig. 9. (Color online) Mode locking results in the case of the 100 μm graphene pattern under high pump power. a) Optical spectrum and b) RF spectrum with oscilloscope trace inset.

Fig. 10. (Color online) Autocorrelation trace of the pulse obtained using a 100 μm graphene pattern.

Fig. 11. (Color online) Mode locking results in the case of the 100 μm graphene pattern under optimized pump power, showing a ps, fundamental frequency pulse. a) Optical spectrum and b) RF spectrum with the oscilloscope trace inset.

Fig. 12. (Color online) Mode locking results in the case of the 150 μm graphene pattern under optimized pump power, showing a broad, fundamental frequency pulse. a) Optical spectrum and b) RF spectrum with oscilloscope trace inset.

Fig. 13. (Color online) Mode locking results in the case of the 150 μm graphene pattern under optimized pump power, showing a ps, fundamental frequency pulse. a) Optical spectrum and b) RF spectrum with the oscilloscope trace inset.

Fig. 14. (Color online) Mode locked pulse spectra using only NPR through the cavity shown in Fig 5(b), for different values of intra-cavity loss, and different pump powers.

Fig. 15. (Color online) Autocorrelation trace of the solely NPR mode locked pulse, under 10 dB intra-cavity loss and using 2 EDFAs. Inset: Oscilloscope trace of the pulse.

Table I. Table comparing the experimental performance metrics of the mode locked fiber laser for different lengths of graphene on a SiN waveguide used inside the cavity.

Length of graphene	Total Loss	Fundamental Mode Locking	Pulse Duration	Spectral 3dB width
100 μm	21.0 dB	Yes	3.51 ps*	1.2 nm
150 μm	22.5 dB	Yes	Unknown	1.1 nm
400 μm	29.2 dB	No	3.37 ps	1.3 nm

*Measured on a higher power multi-pulse output

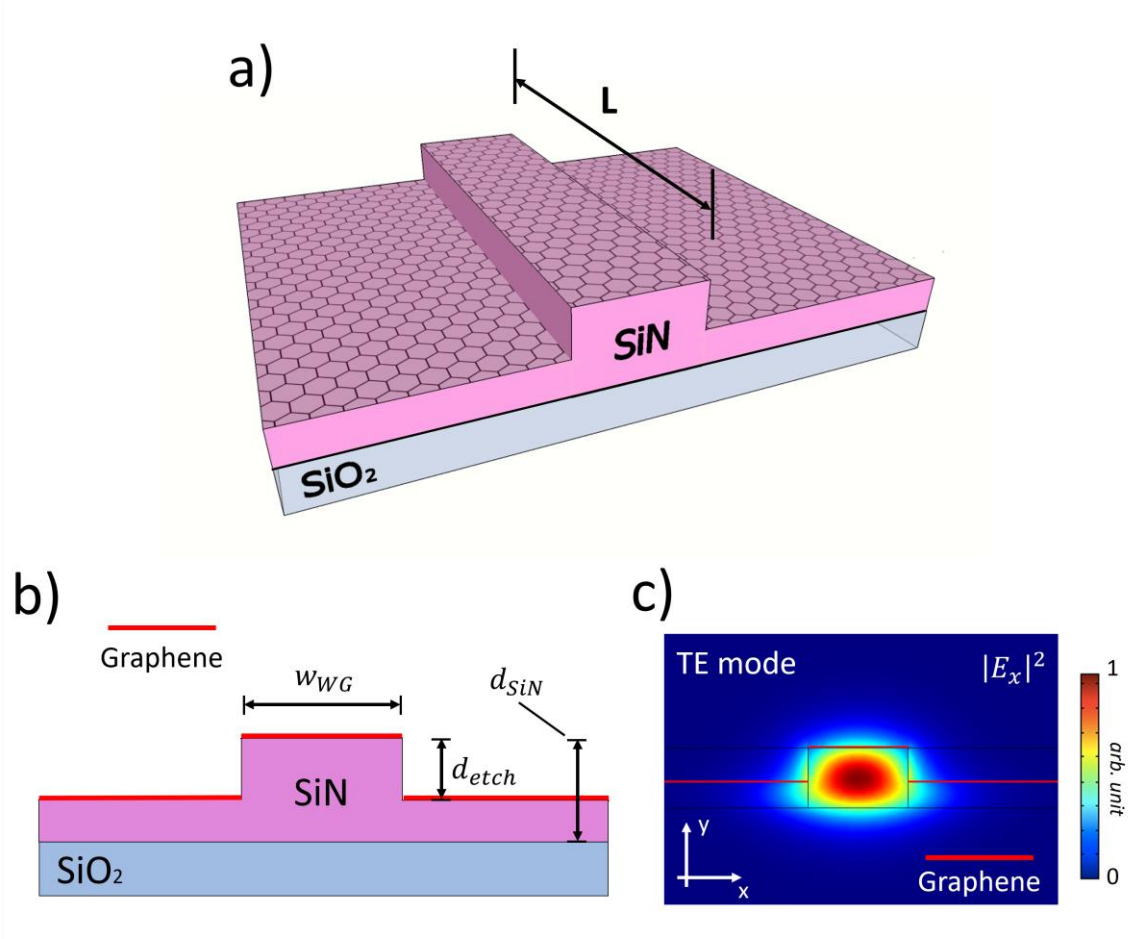

Fig. 1. (Color Online)

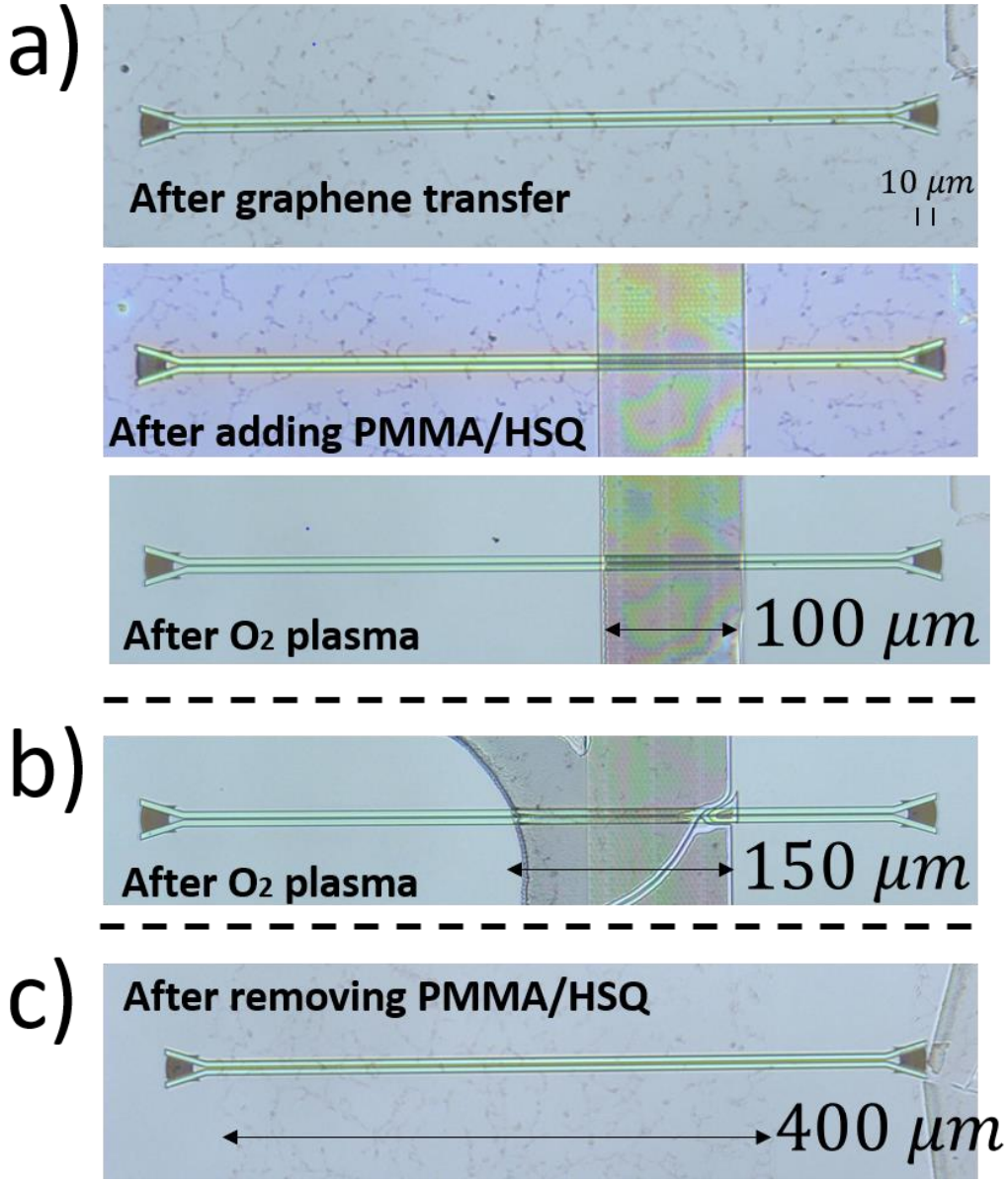

Fig. 2. (Color Online)

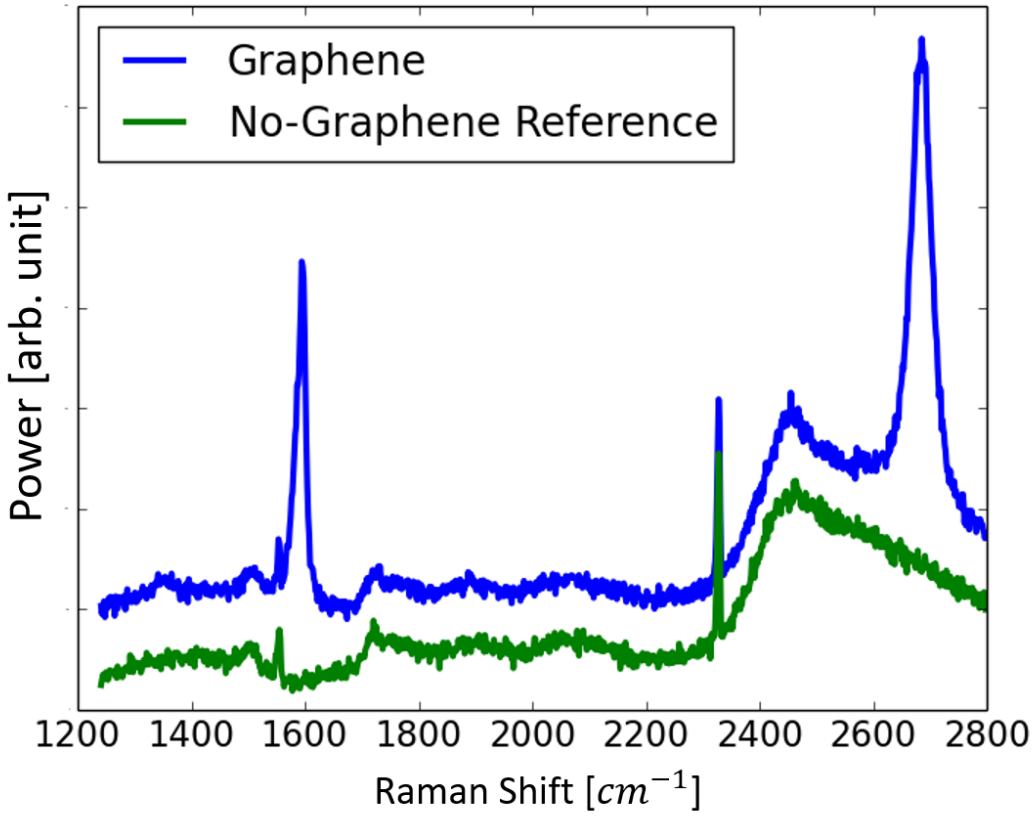

Fig. 3. (Color Online)

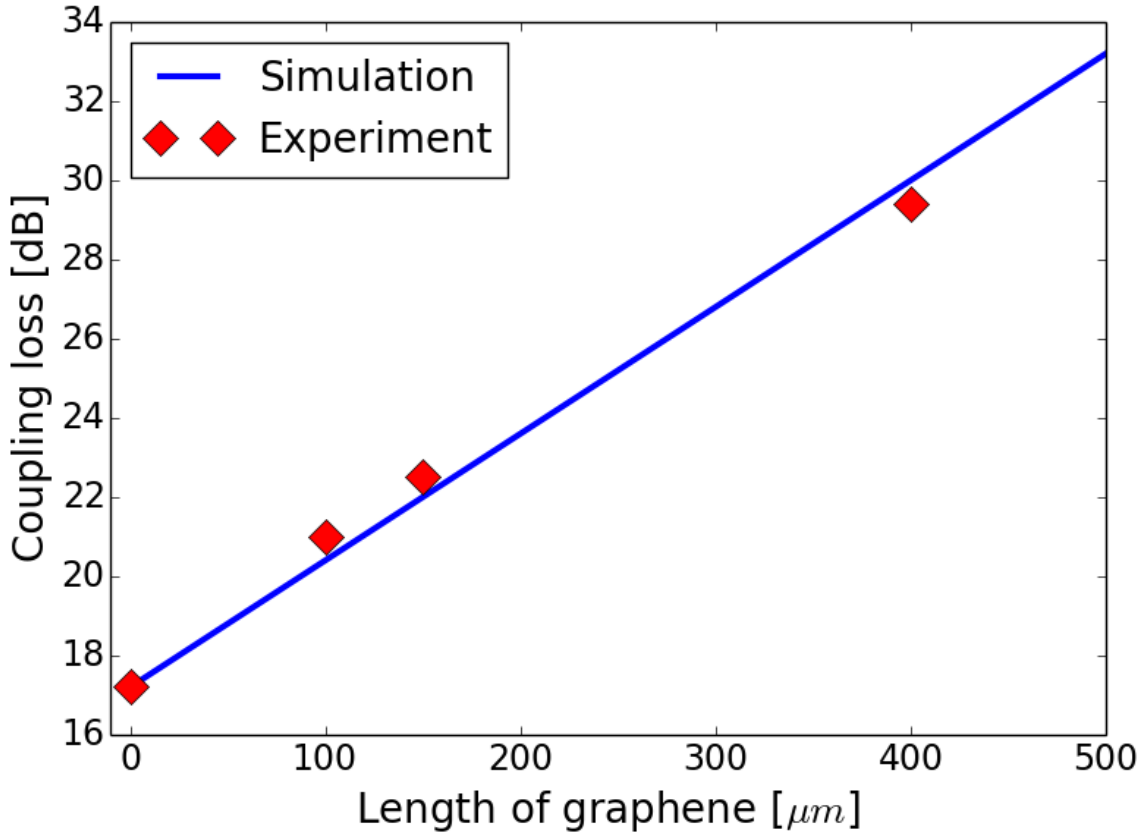

Fig. 4. (Color Online)

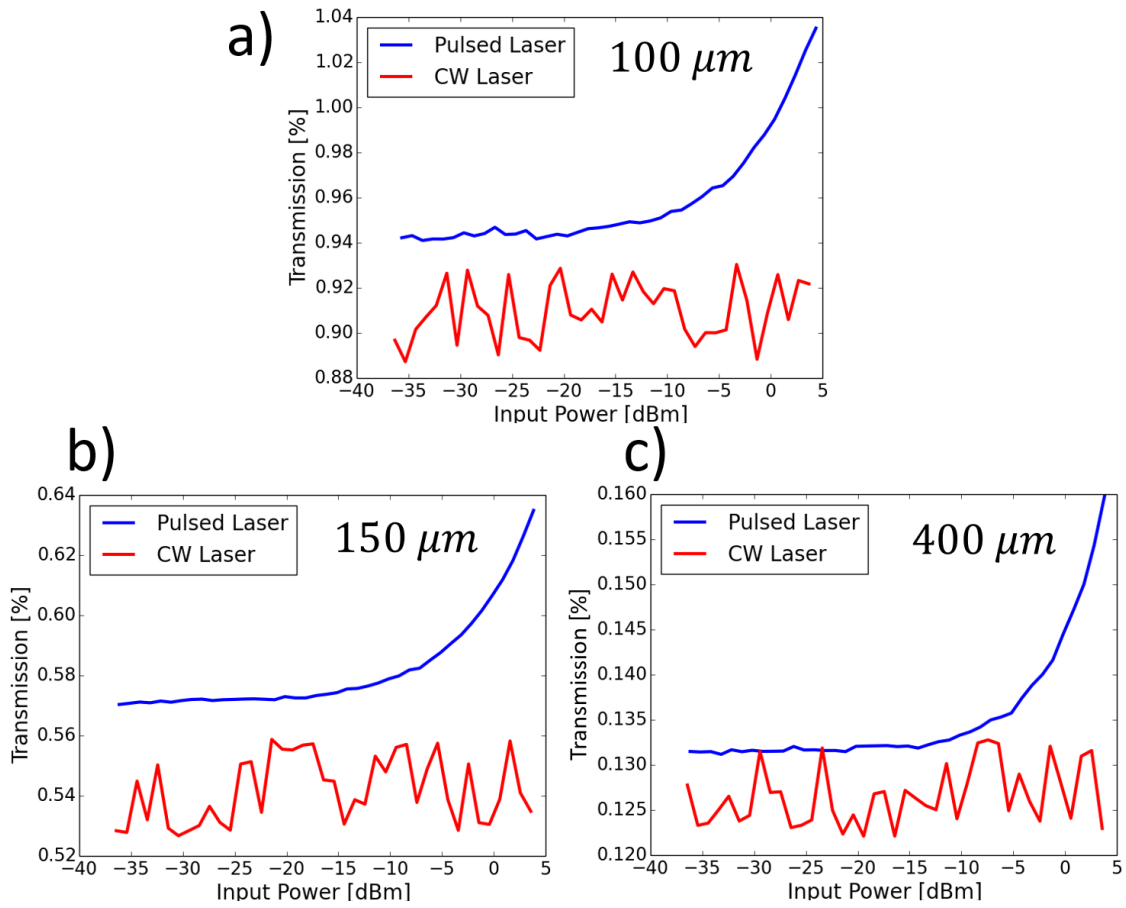

Fig. 5. (Color Online)

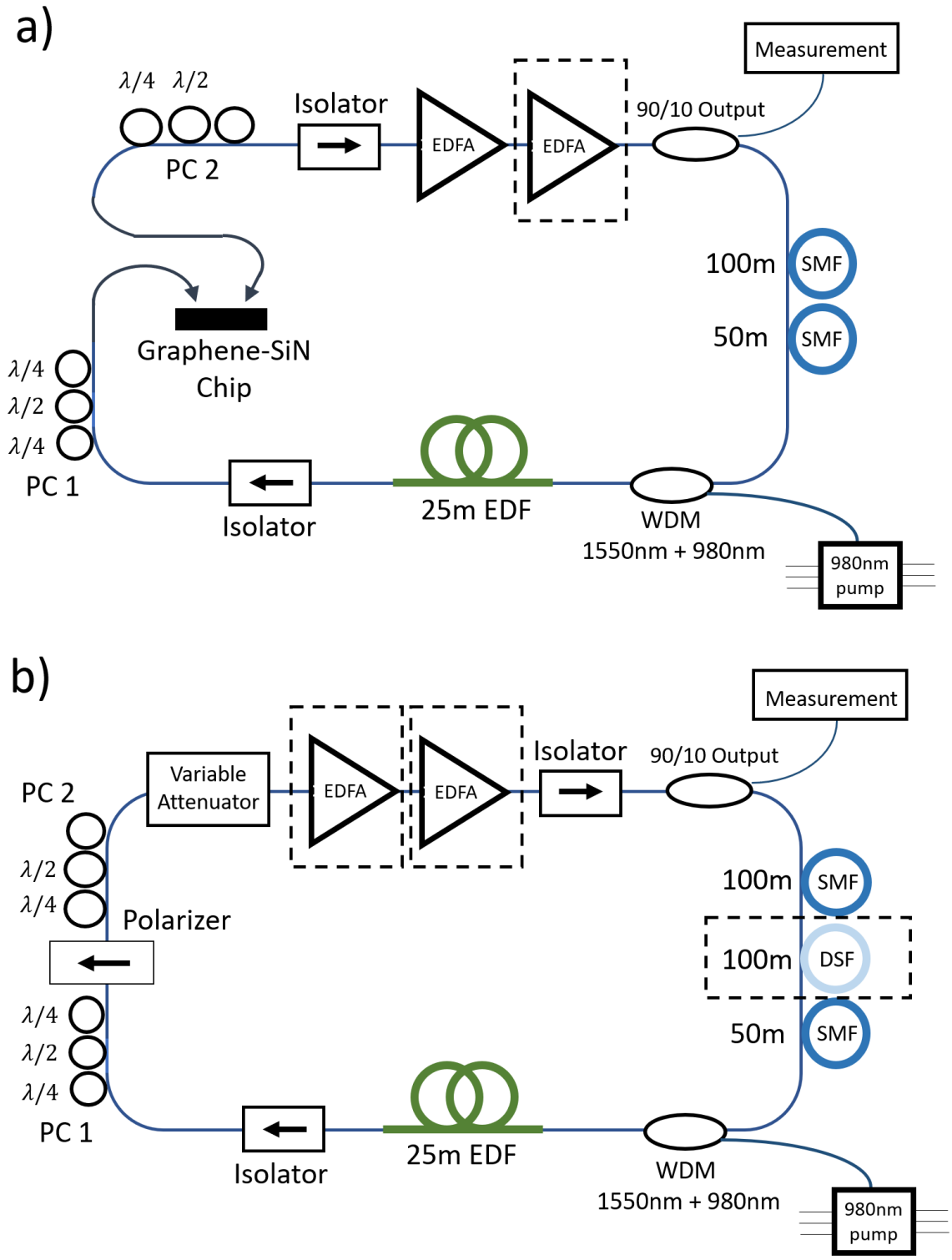

Fig. 6. (Color Online)

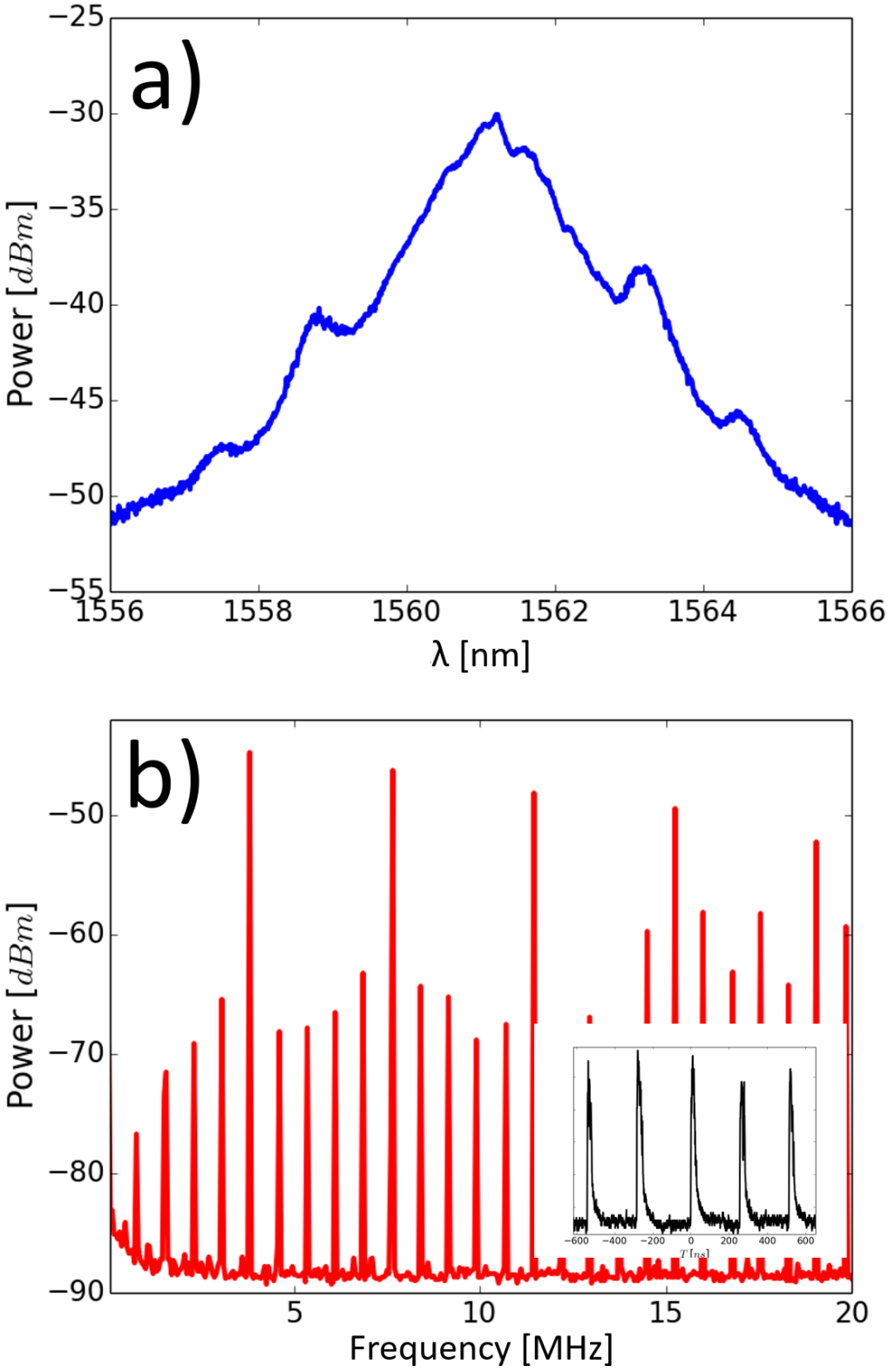

Fig. 7. (Color Online)

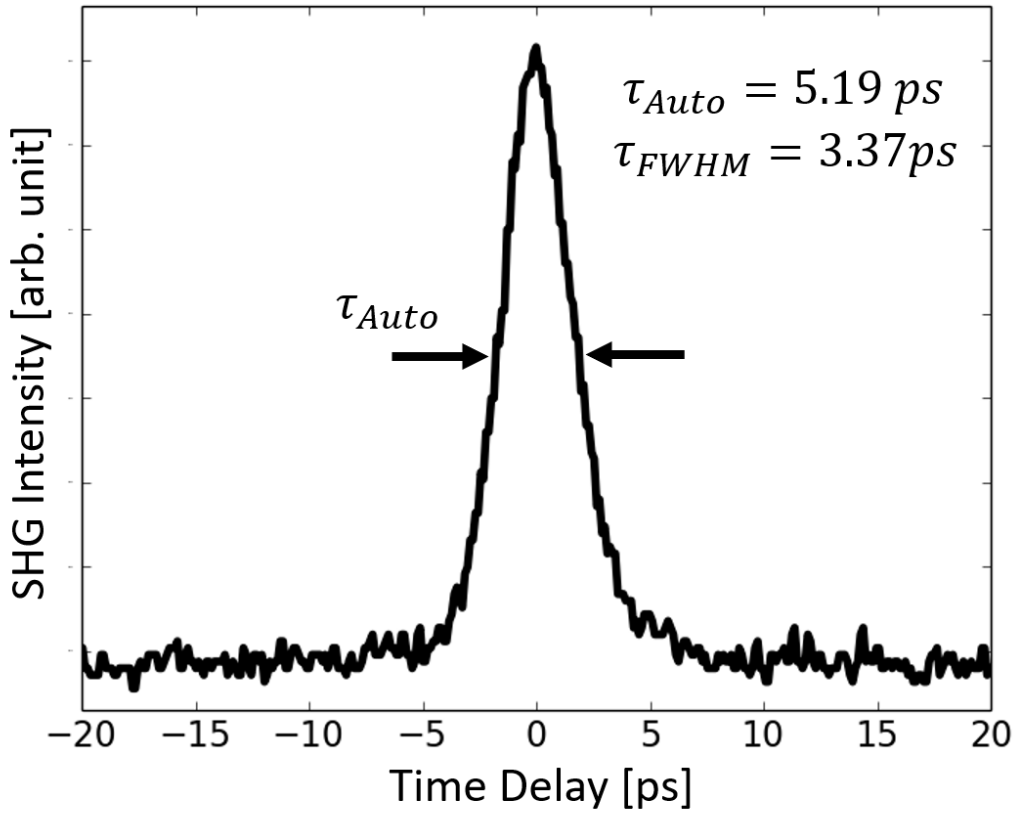

Fig. 8. (Color Online)

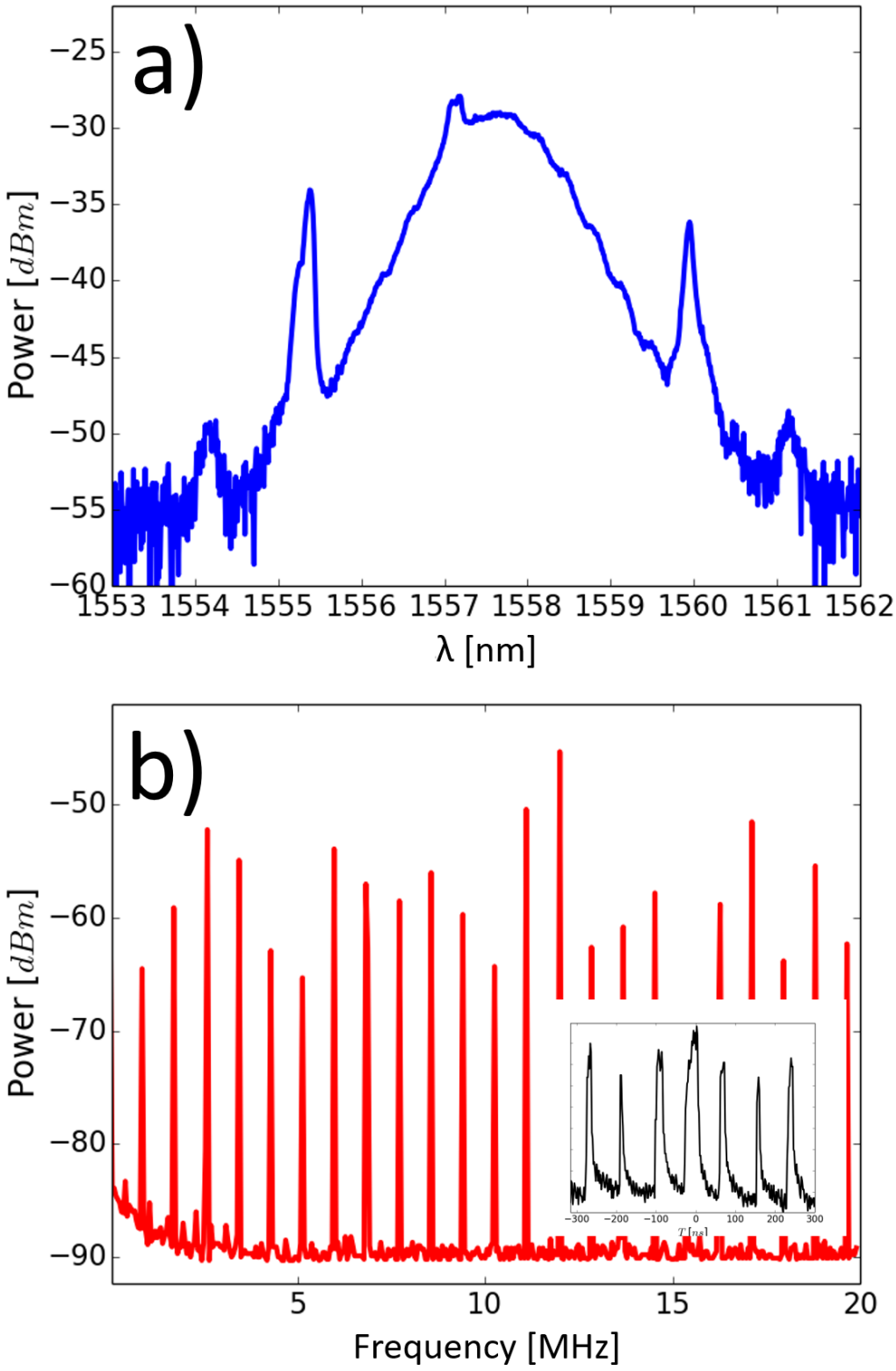

Fig. 9. (Color Online)

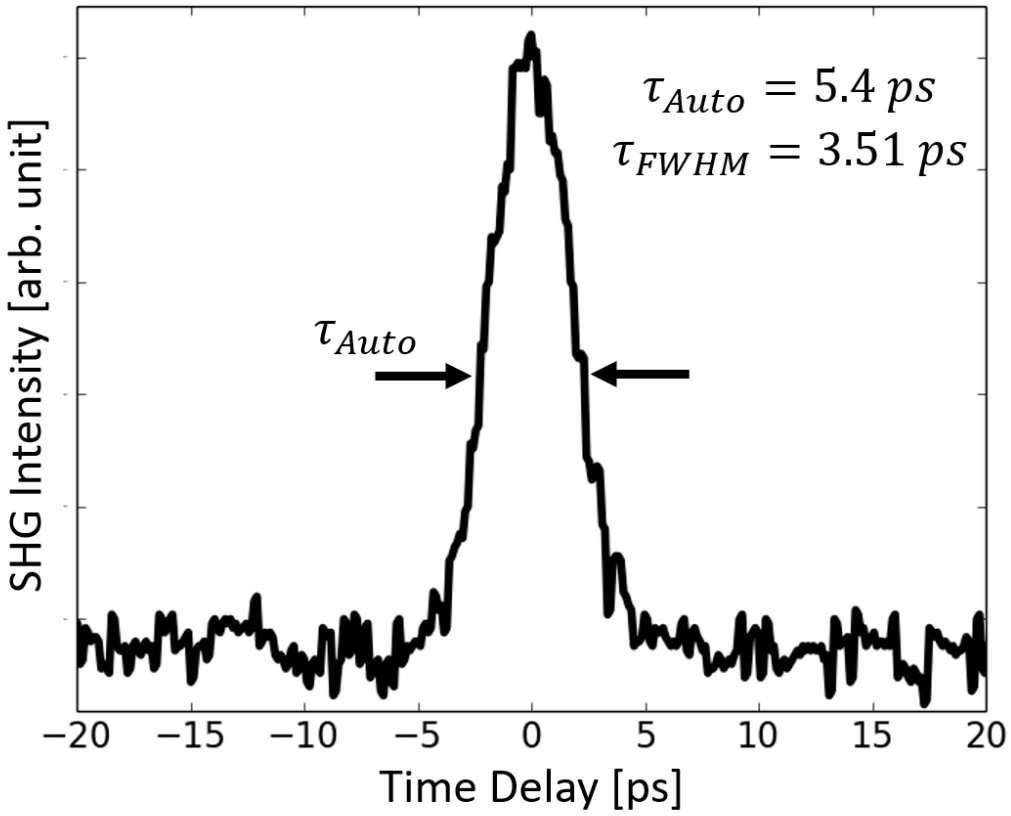

Fig. 10. (Color Online)

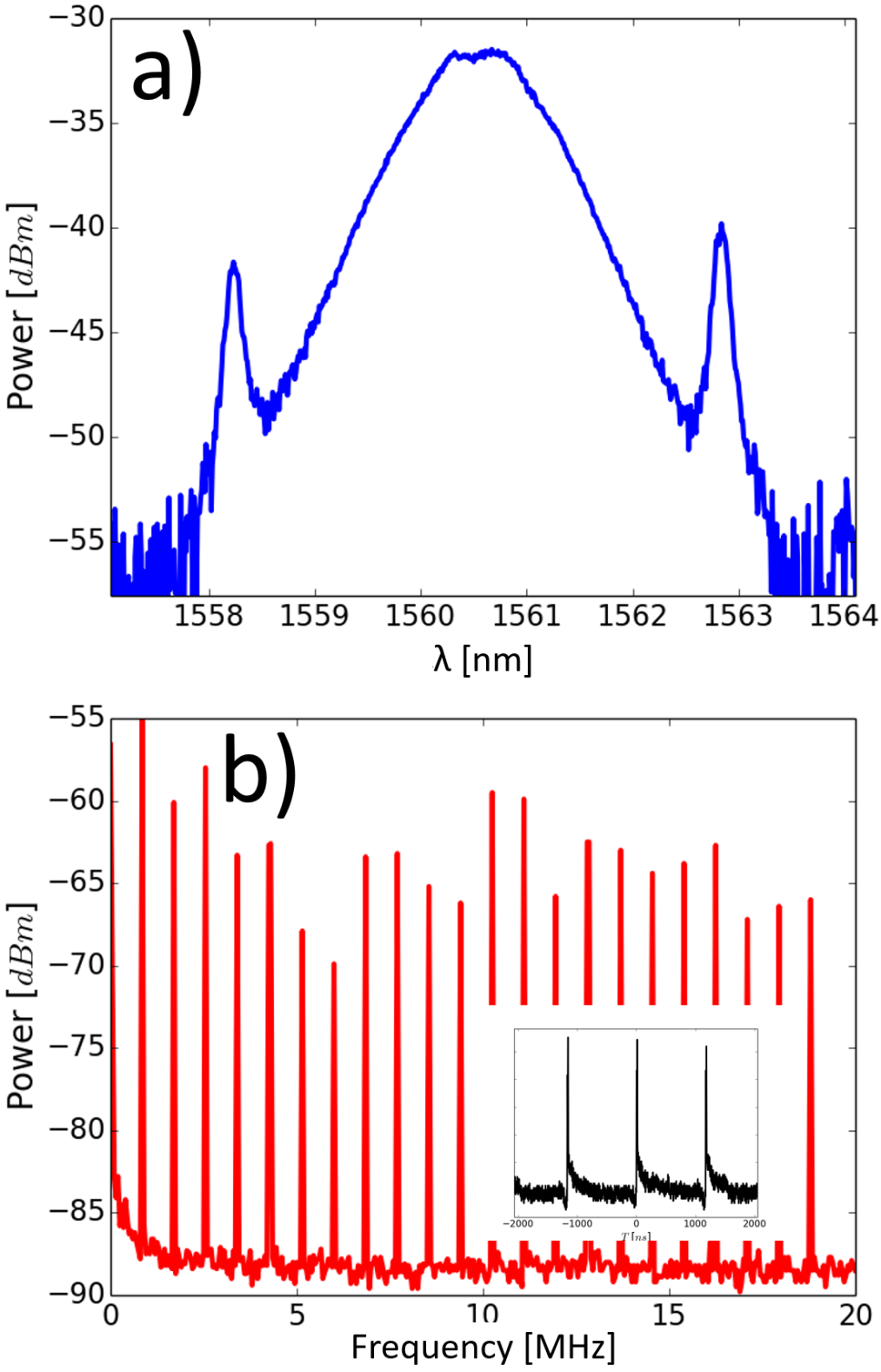

Fig. 11. (Color Online)

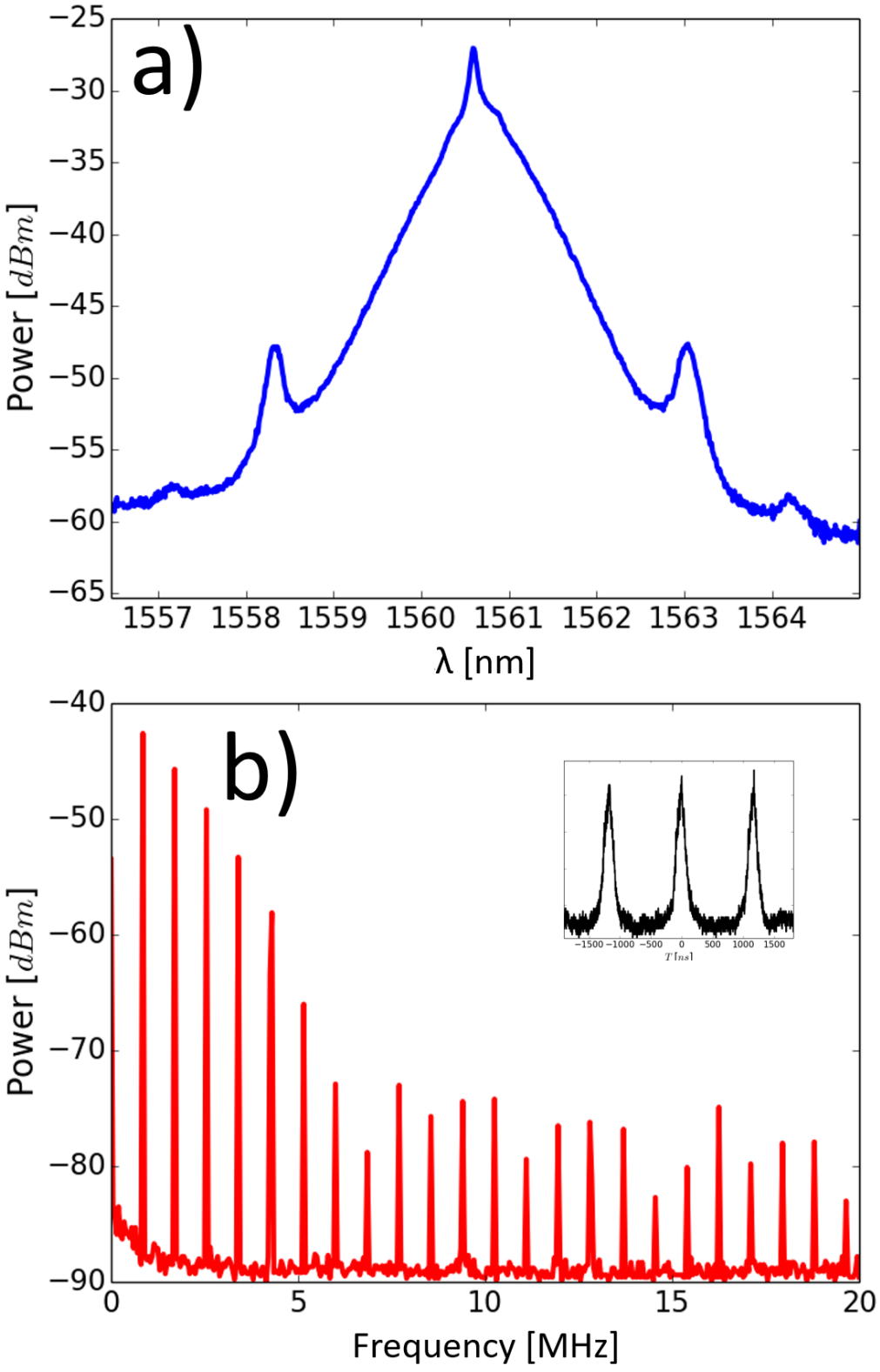

Fig. 12. (Color Online)

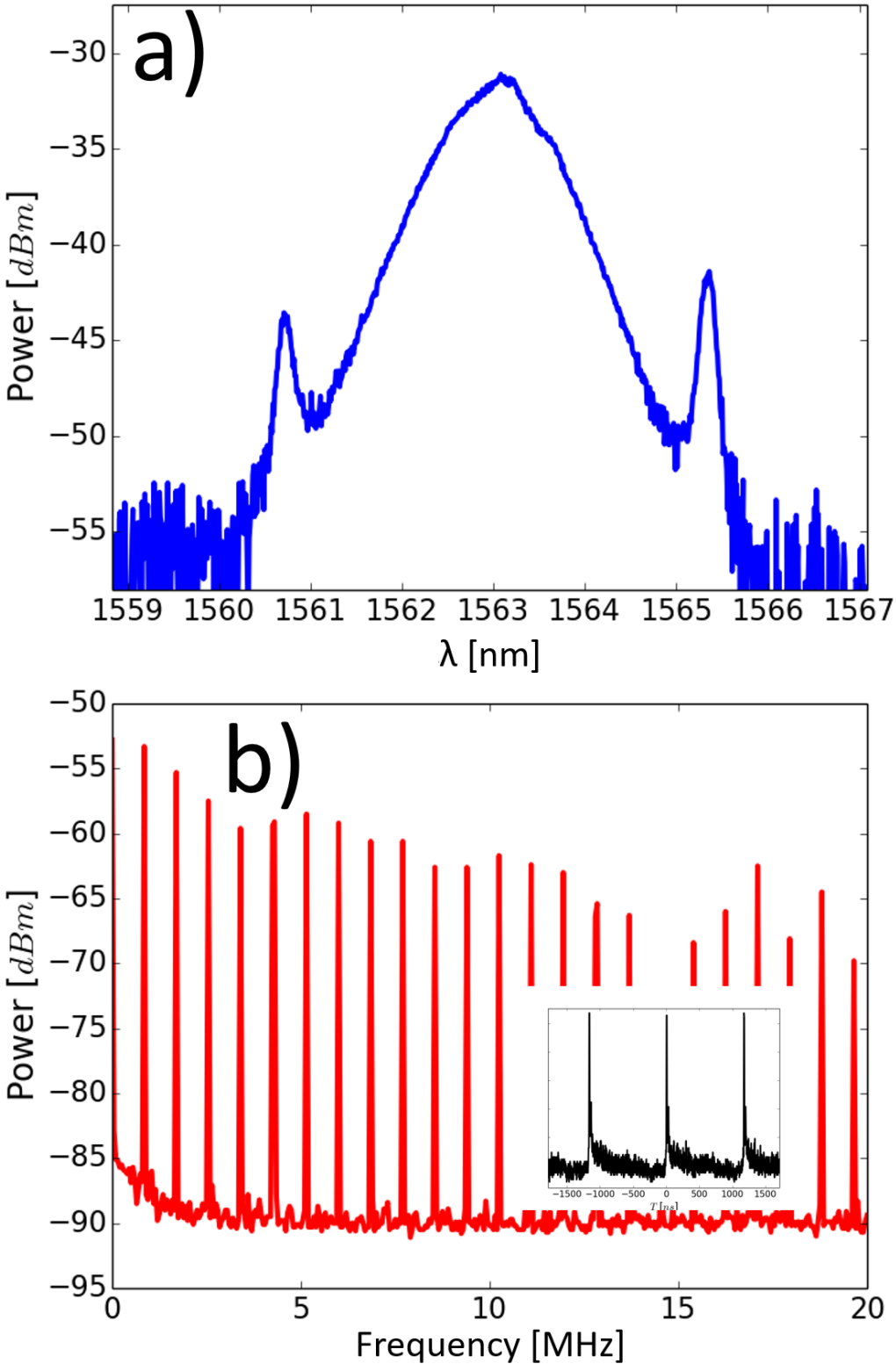

Fig. 13. (Color Online)

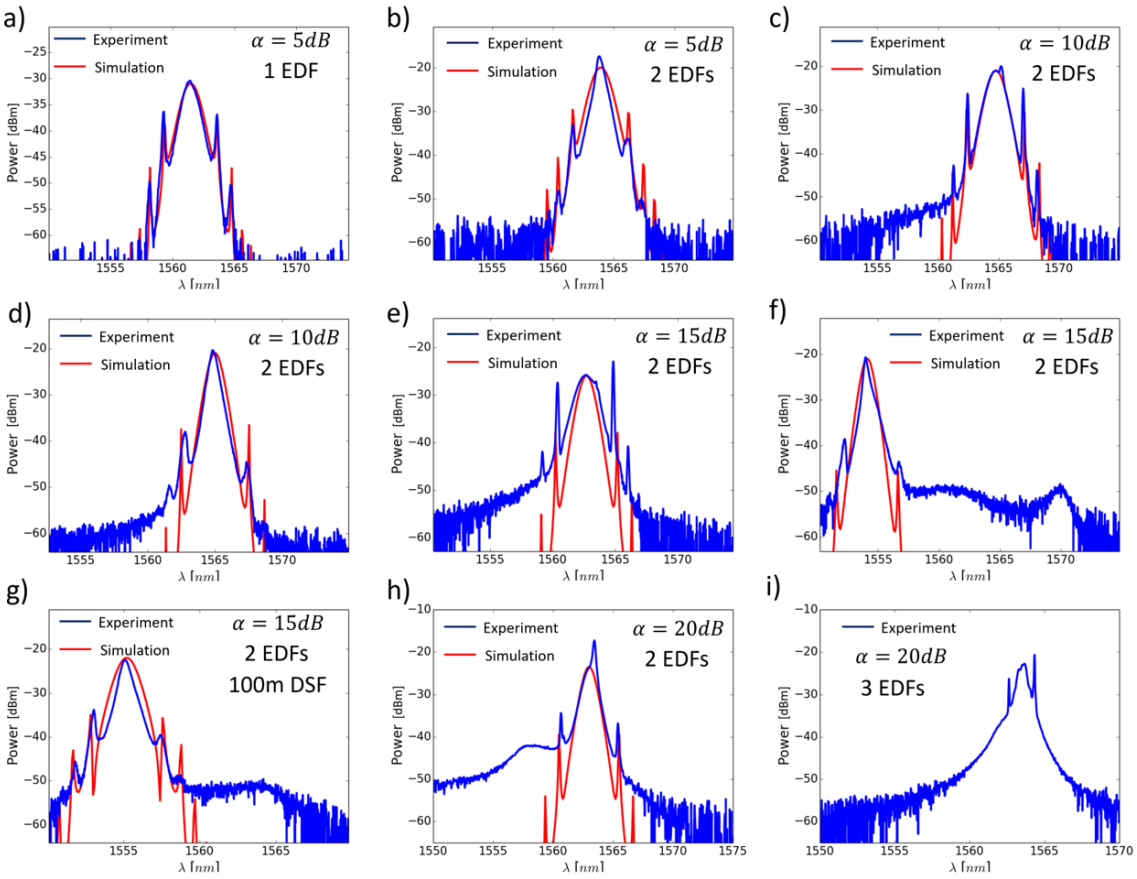

Fig. 14. (Color Online)

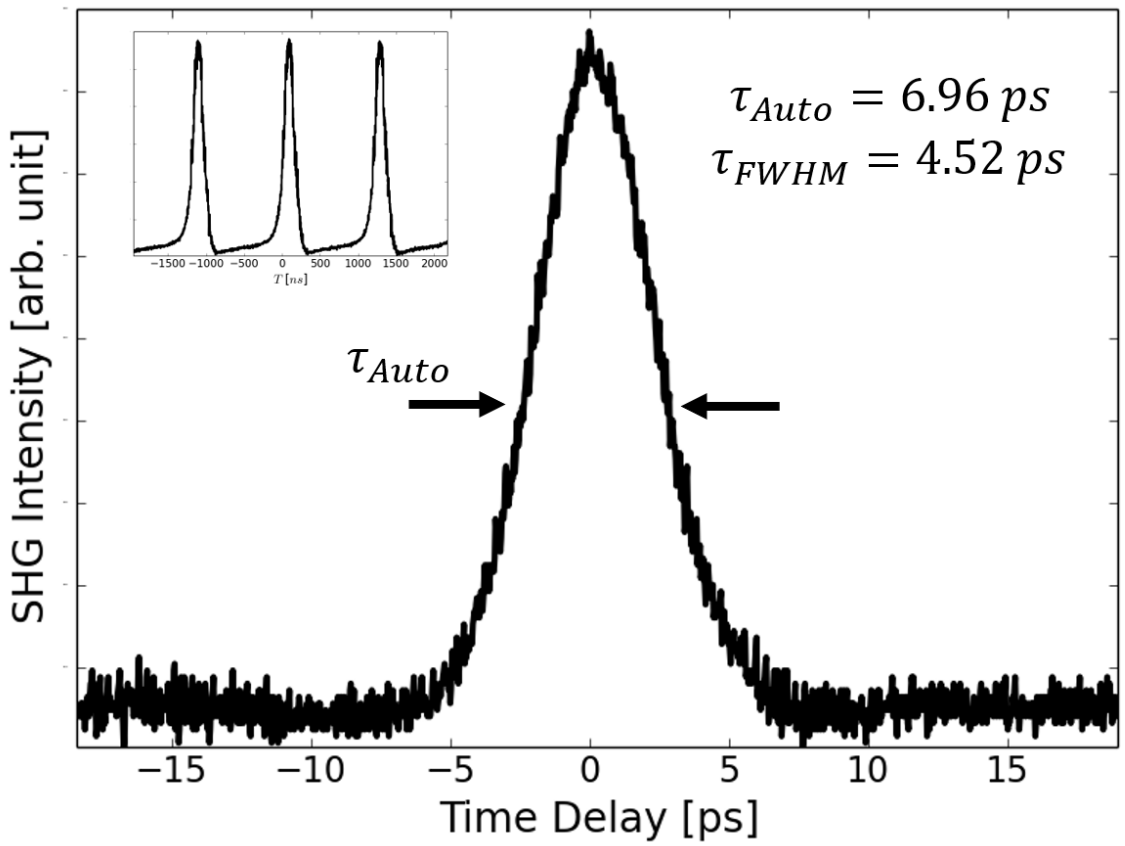

Fig. 15. (Color Online)